Electronic Structures and Photoconversion Mechanism in Perovskite/Fullerene Heterojunctions

Ming-Fai Lo, Zhi-Qiang Guan, Tsz-Wai Ng, Chiu-Yee Chan, and Chun-Sing Lee**

It has been generally believed and assumed that organometal halide perovskites would form type II P–N junctions with fullerene derivatives (C_{60} or PCBM), and the P–N junctions would provide driving force for exciton dissociation in perovskite-based solar cell. To the best of our knowledge, there is so far no experiment proof on this assumption. On the other hand, whether photogenerated excitons can intrinsically dissociate into free carrier in the perovskite without any assistance from a P–N junction is still controversial. To address these, the interfacial electronic structures of a vacuum-deposited perovskite/C_{60} and a solution-processed perovskite/PCBM junctions is directly measured by ultraviolet photoelectron spectroscopy. Contrary to the common believes, both junctions are found to be type I N–N junctions with band gap of the perovskites embedded by that of the fullerenes. Meanwhile, device with such a charge inert junction can still effectively functions as a solar cell. These results give direct experimental evidence that excitons are dissociated to free carriers in the perovskite film even without any assistance from a P–N junction.

1. Introduction

Organometal halide perovskites materials such as $CH_3NH_3PbI_3$, $CH_3NH_3PbI_{3-x}Cl_x$, and $CH_3NH_3PbBr_3$ have recently aroused much interest in photovoltaic applications because of their impressive performance.[1–4] Despite tremendous efforts devoted on materials processing and device architecture design, current knowledge on their photocharge generation mechanisms in solar cells are limited.[5–8] Interfacial energetics and charge interactions at their contacts with neighboring materials are crucial factors influencing device performance. However, there is so far few reports on the surface energy-band structures and interfacial charge interactions of perovskites with their neighboring films.[6,9]

Dr. M.-F. Lo, Mr. Z.-Q. Guan, Dr. T.-W. Ng, Miss C.-Y. Chan, Prof. C.-S. Lee
Center of Super-Diamond and Advanced Films (COSDAF)
Department of Physics and Materials Science
City University of Hong Kong
Hong Kong SAR, P. R. China
E-mail: tszwaing@cityu.edu.hk; apcslee@cityu.edu.hk
Dr. M.-F. Lo, Dr. T.-W. Ng, Prof. C.-S. Lee
City University of Hong Kong Shenzhen Research Institute
Shenzhen, P. R. China

DOI: 10.1002/adfm.201402692

Perovskite materials were initially used as photons absorbers and/or sensitizers sandwiched between TiO_2 (N-type) and Spiro-OMeTAD (P-type) to form P-i-N structures.[10–12] After discovery of their good hole-transporting capabilities, perovskite materials are later widely utilized also as a P-type semiconductor forming P–N junctions with TiO_2 or fullerene (e.g., C_{60}, PCBM etc).[13–15] These P–N heterojunctions are generally considered to provide driving force for charge separation. However, some recent studies revealed that organohalide lead perovskites have small exciton binding energies of 37–50 meV and that bulk exciton dissociation might be possible under thermal excitation at room temperature (≈26 meV) without assistance from a P–N junction.[16] Recently, Friend and co-workers[17] showed that long-lived free charges can be formed in perovskite at room temperature. Nevertheless, charge separation mechanisms in these materials are still controversial and this might hinder further development of the perovskite-based solar cells.[18,19]

Currently, exciton dissociations in perovskite-based devices are frequently discussed by considering P–N junctions formed between perovskites and their neighboring layers.[13,15,20–22] In particular, a donor–acceptor heterojunction of type II with a staggered gap is generally assumed for enabling/enhancing charge dissociation at the P–N junction.[15,23–25] In fact, so far there is no experiment proof for the P–N junction assumption for typical contacts between organometal halide perovskites and fullerene derivatives. In this work, we directly measured electronic energy-band structures of both a vacuum-deposited $CH_3NH_3PbI_{3-x}Cl_x$/ C_{60} and a solution-processed $CH_3NH_3PbI_3$/ PCBM junctions with ultraviolet photoelectron spectroscopy (UPS). Contrary to the widely used type II P–N junction assumption, both junctions were found to be type I N–N junctions in which the valence and conduction band (CB) edges of the perovskite are bracketed by the highest occupied molecular orbit (HOMO) and LUMO of the fullerenes. Albeit with the charge inert $CH_3NH_3PbI_{3-x}Cl_x/C_{60}$ interfaces, device with the configuration of indium tin oxide (ITO)/$CH_3NH_3PbI_{3-x}Cl_x$/ C_{60}/Bphen/Al does show reasonable solar cell performance. As these type I junctions do not provide any driving force for exciton dissociation, these results present clear experimental evidence that charge dissociation is effectively taken place in the perovskite film with free carrier generation even without any assistance from a P–N junction.

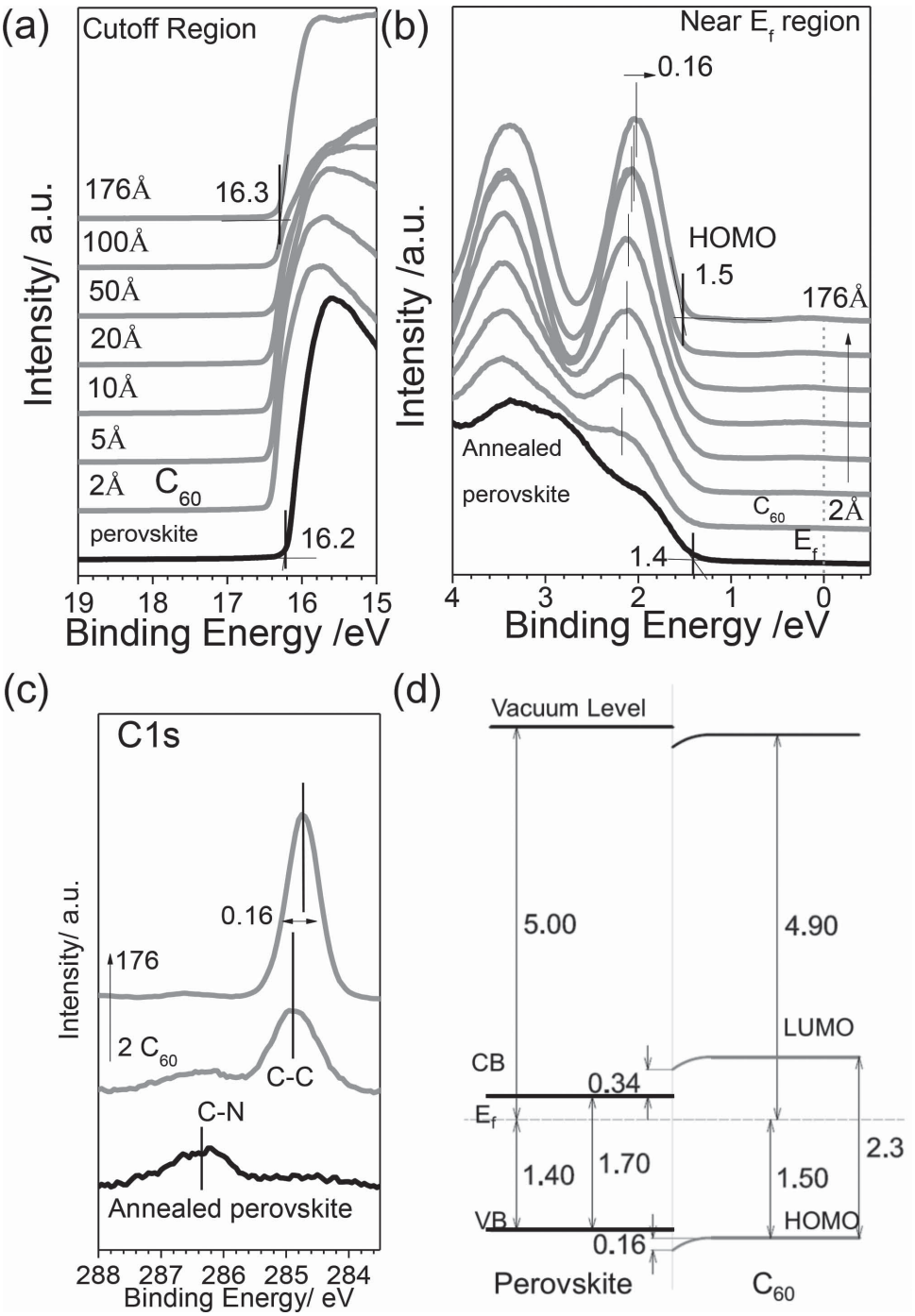

Figure 1. UPS (He I) spectra of a) the cutoff region and b) the near E_f region as a function of increasing C_{60} deposition on ITO/ perovskite substrate. c) The XPS C1s core levels spectra of C_{60} (gray lines) deposition on ITO/annealed perovskite substrate (black line). d) The interfacial electronic band structure of perovskite/C_{60} interface.

2. Results and Discussion

To look into details of charge interaction at a perovskite/C_{60} junction, its interfacial energetics and bands structure were examined using UPS and X-ray photoemission spectroscopy (XPS). The perovskite film is mainly prepared by thermal evaporation. Its purity and crystalline structure are characterized with results shown in Figure S1 (Supporting Information), which is comparable to others.[2,26] In particular, the perovskite films show a XRD peaks at 14°, 28°, and 43° that correspond to (110), (220), (330), respectively.

Figure 1a,b show UPS spectra of in situ-prepared C_{60} deposited on an ITO/perovskite substrate. The secondary electron cutoff position of the pristine perovskite film prepared on ITO

substrate is located at 16.2 eV (bottom line, Figure 1a); while its onset of the valence band maximum is found at 1.4 eV (bottom line, Figure 1b). Strong signal attenuation was observed in the valence features of the perovskite even at a low C_{60} coverage of 2 Å. The secondary electron cutoff of C_{60} is located at 16.3 eV, indicating a downshifted of vacuum level for 0.1 eV. Figure 1b also shows a slight shift in the HOMO peak of 0.16 eV. This shift matches well with that observed in the XPS C1s core level peak as shown in Figure 1c. The C peak observed at 284.8 eV, corresponds to C—C bond in C_{60}, shows a shift of 0.16 eV when the thickness of C_{60} increase from 2 to 176 Å. Meanwhile, another C peak located at 286.3 eV corresponds to C—N bond signal from the underlying perovskite shows rigid shift. Peak shifts in HOMO and C signals of C_{60} are attributed to its molecular energy level bending of C_{60} during contact formation with perovskite. The above results are summarized as an energy level diagram as shown in Figure 1d. It can be seen that the Fermi level lies close to the CB edge of the perovskite indicating a strong N-type characteristics of perovskite films. This result is consistent to other reports.[6,9,27] The perovskite/C_{60} junction shows a distinct N–N junction instead of a presumed P–N junction. The band gap of the perovskite is within that of C_{60}, showing a type I junction with straddling gap. Contrary to charge interactive type II junction commonly observed in P–N solar cell devices, a type I junction is electronically inert and carries no charge interaction in vicinity of the forming junction. It cannot provide any driving force to separate the photogenerated charges. In short, the experimental results are contrary to the common believes that perovskite/fullerene junctions are 1) type II P–N junctions and; 2) would thus assist electron–hole separation.

The energy-band structure of the perovskite/C_{60} junction is unexpected. It is important to know whether the above result is just a unique case to perovskite/C_{60} junction prepared in vacuum. To answer this question, the experiment was repeated for a perovskite/fullerene junction prepared entirely by solution processing. A $CH_3NH_3PbI_3$/PCBM junction was prepared by spin coating and the corresponding UPS spectra and energy level diagram are shown in **Figure 2**. XRD data of the prepared perovskite films is shown in Figure S2, Supporting Information. The XRD signal of solution-processed perovskite films is similar to that thermal-evaporated perovskite film showing observable signals at (110), (220), and (330). Figure 2a,b show UPS spectra of ≈5 and ≈100 Å PCBM thick films spin coated on an ITO/perovskite substrate. The ionization potential of PCBM is ≈6 eV which is consistent to previous reports.[28,29] Upon coating of ≈5 Å PCBM on the perovskite film, the secondary electron cutoff position of the UPS spectra slightly shifted by 0.25 eV toward the high binding energy side. Further increasing the PCBM thickness causes no additional shifts in both the cutoff and the onset of the UPS spectra. UPS results of the solution-processed perovskite/PCBM junction are summarized as an energy level diagram in Figure 2c. Due to the energy-band offset at the vacuum levels at the perovskite/PCBM interface, the HOMO of PCBM becomes align with the VB of the perovskite film. This result in an energy-band structure similar to that of the vacuum-deposited perovskite/C_{60} junction, showing a charge inert type I junction. The UPS results in Figures 1 and 2 are consistent with each other, suggesting perovskite/fullerene contacts are N–N type I junctions irrespective to vacuum or solution processing.

This is the first time observation that the perovskite/C_{60} junction behaves as an isotype (N–N) junction. Organometal halide perovskites are known to be sensitive to the processing conditions in particularly moisture, solvent, preparation environment etc.[30,31] To eliminate unnecessary environmental variables that might affect the charge interaction of the testing perovskites film, experiments were in situ carried out in vacuum, with the perovskite prepared by thermal coevaporation of methylammonium iodide (MAI) and $PbCl_2$ (see Experimental Section). The prepared perovskite films were carefully characterized in order to rule out any side effects due to undesirable contaminants that might affect the electronic structure and charge distribution. The XPS is used to monitor the elemental changes at perovskite/C_{60} and perovskite PCBM interfaces (see Figure S3 and S4, Supporting Information). When C_{60} (or PCBM) is deposited on the perovskites film, a sharp C peak is emerged at a position of 285 eV. This is referred to the C—C bond of deposited C_{60} (or PCBM). Apart from the C signal, the spectra of Pb 4f, N 1s, and I 3d show negligible change in both spectral shape and peak position. This indicates that there is no chemical interaction takes place at the solution-processed perovskite/PCBM junction. To consolidate our suggestion, the UPS experiment is further repeated using Si (Figure S5, Supporting Information) and FTO (Figure S6, Supporting Information) substrates with work function of 3.91 and 4.28 eV, respectively. Similar N–N type I junctions are observed no matter what substrates are used.

In order to understand the charge interaction and transporting properties, the perovskite/C_{60} interface was studied using photoluminescence (PL) spectroscopy. **Figure 3**a shows steady-state PL spectra of 125 nm thick perovskite deposited on Si substrate (black solid line). The sample exhibits a PL emission peak at ≈780 nm which is similar to that reported in literature.[26] When 40 nm of C_{60} film is deposited on top of the perovskite film, PL quenching is observed. Such PL quenching result can be due to (1) exciton dissociation at the perovskite/C_{60} junction; or (2) free carriers removal from perovskites film.[22] From our UPS data, we showed that the perovskite/C_{60} is a type I N–N junction that has no driving force for charge separation. Therefore, the PL quenching can only be due to the carrier transport from perovskite to C_{60}. The photogenerated free carriers (or weakly bound excitons) in perovskite can no longer be radioactive decayed to ground state after its contact with C_{60}. Both UPS and PL results confirmed the effective electron extraction from perovskite to C_{60}. The instant charge transfer at perovskite/C_{60} results in observable band bending in C_{60} that further reduce the electron-transporting barrier to only ≈0.3 eV. Such energy barrier is small enough to allow efficient charge exchange crossing the pervoskite/C_{60} interface even though the contact is of type I.

A simple device with a configuration of ITO/$CH_3NH_3PbI_{3-x}Cl_x$(150 nm)/C_{60} (40 nm)/Bphen (8 nm)/Al layer was fabricated. The chemical structure of forming perovskite used for device fabrication is also examined using both XPS (Figure S7, Supporting Information), with results identical to that in Figure S3 (Supporting Information). They both have I:Pb ratio of ≈3:0. External quantum efficiency (EQE) and current density–voltage (J–V) characteristics of the device are shown in Figure 3. Figure 3b shows that photocurrent generation begins at 790×10^{-9} m, which is in good agreement with the band gap of the perovskite film.[26,32] The EQE spectrum later reaches a

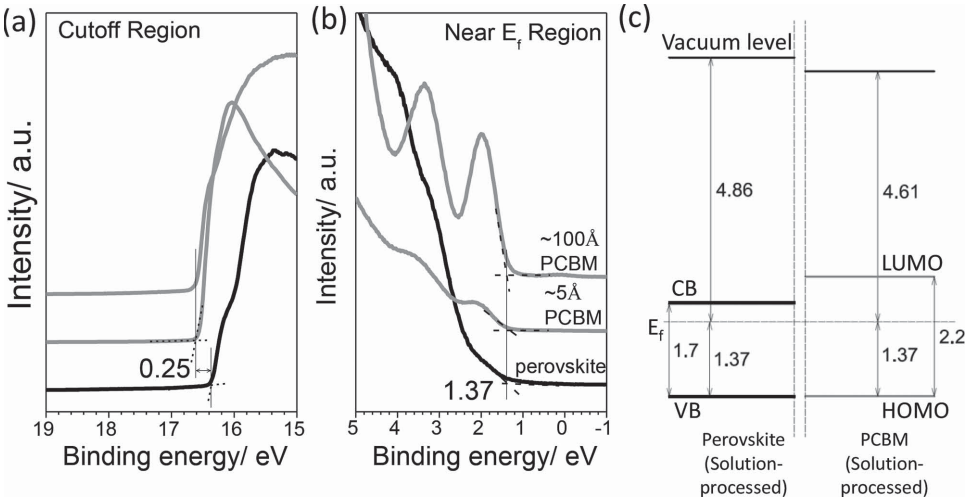

Figure 2. UPS (He I) spectra of a) the cutoff region and b) the near E_f region of an ITO/ perovskite substrate with 5 and 100 Å of PCBM on top. c) The energy-band structure of perovskite/PCBM showing a straddling gap with charge noninteractive interface. Due to the nature of spin coating, it is difficult to prepare uniform PCBM films with precise thickness less than 5 Å. Changes in energy levels within the first 5 Å of PCBM were not measured and thus energy levels in the region were not shown between the two vertical dashed lines at the perovskite/PCBM interface.

peak value of 80% in the short-wavelength visible region. It has to mention that the perovskite is prepared by simple coevaporation, a decrease in EQE in long wavelength region of the spectrum is observed.[3] The device shows an open circuit voltage (V_{oc}) of 0.79 V, a short-circuit current (J_{sc}) of 13.2 mA cm^{-2}, a fill factor of 0.62 and a power conversion efficiency of 6.42% (Figure 3c). While the efficiency is lower than that of the state-of-the-art perovskite solar cells, it is worth mentioning that the present simple device does not use any mesoporous scaffold structure, hole transporter (e.g., spiro-OMeTAD) nor a hole injecting layer (e.g., PEDOT:PSS) for performance enhancement.[14,33] In fact, the efficiency of the present device is among the highest obtained in perovskite/fullerene-based solar cells prepared entirely with thermal evaporation.

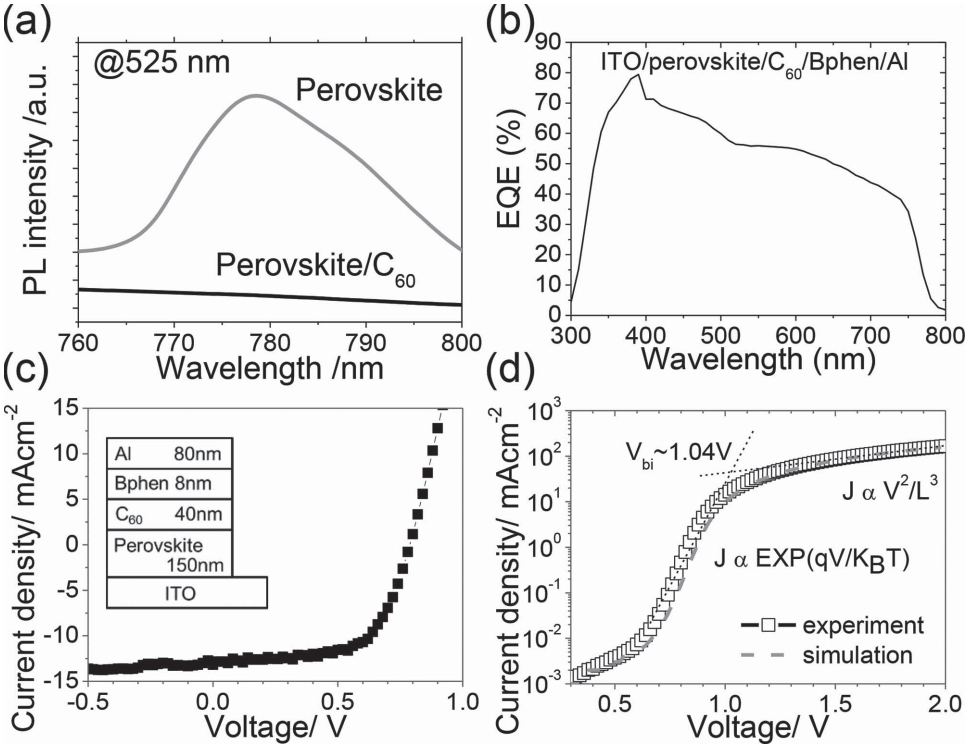

Figure 3. a) PL emission of Si/perovskite and Si/Perovskite/C_{60} measured under excitation energy 525 nm. b) EQE spectra and c) *I–V* curve under 1 sun and d) dark *I–V* curve of perovskite-based device prepared by thermal evaporation process with a structure of ITO/ perovskite (150 nm)/C_{60} (40 nm)/ Bphen (8 nm)/Al measured. The dark current fitting result is shown as dashed lines in (d).

It is widely observed that the V_{oc} of perovskite/C_{60} device is < 1 V. In order to understand the device behavior, the dark *I–V* characterizes in Figure 1c is fitted using the diode equation. We obtained an ideality factor (n) = 3.64, and the saturated dark current (J_d) = 8.73 × 10^{-4} mA cm^{-2}. The ideality factor of perovskite/C_{60} device are far from ideal (i.e., P–N diode characteristics), much worse than values typically obtained from organic solar cell materials ($1 < n < 2$).[34,35] Furthermore, the *V*oc calculated using the dark current fitting parameter is 0.85 V, which is very close to the measured value (0.79 V) at one sun.

At low voltage (<0.7 V), the measured current is dominated by local leakage current. In the range of 0.7–1.1 V, the current exponentially increase with increasing voltage. In this regime the current is dominated by diffusion. When the flat-band condition is reached, the current becomes space-charge limited (i.e., SCLC current).[36] Consequently, the build-in voltage (V_{bi}) can be read at the cross point between the exponential region and SCLC regime, which is ≈1.04 V. This value can be taken as an upper limit for *V*oc in this device. This V_{bi} value is 0.3 eV larger than the measurable V_{oc} (i.e., 0.79 eV in Figure 3c). The 0.3 eV V_{oc} loss is well matched with the energy-band offset between CB of perovskite to the LUMO of C_{60} (i.e., ≈0.3 eV)

Nevertheless, the most important message from Figure 3b is that photogenerated excitons can effectively dissociate even in the absence of a P–N junction. These results provide clear evidence that free carriers can be intrinsically generated within the perovskite absorber upon photoexcitation. Photovoltaic conversion in the perovskite/fullerene system is in fact analogous to that in the AlGaAs/GaAs system.[37] Upon photoexcitation, the perovskite film acts as an intrinsic absorber with high electronic quality that generates excitons with low binding energies of 50 meV and can be readily dissociated.[38] In short, the present results provide strong evidence indicating direct charge separation within the perovskite absorber layer itself.

3. Conclusion

While it is commonly believed that perovskite/C_{60} solar cell shares a similar photocharge generation mechanism as common organic solar cells with type II P–N junctions. Our photoemission results showed that perovskite/C_{60} interfaces in fact behave as charge noninteractive type I N–N junctions. These results give direct evident that a perovskite/C_{60} interface does not provide driving force for the charge dissociation process. A device with such a junction is therefore operated by instant charge dissociation with generated free carriers in the perovskite film. Further device optimization and improvement requires a deeper knowledge on the functionality and charge control at perovskite/fullerene junctions. Our results give an important step forward by showing the charge energetics at simple planar perovskite-based devices, and provide guidance for future device design.

4. Experimental Section

Photoemission Studies: Photoelectron spectroscopies were carried out with a VG ESCALAB 220i-XL surface analysis system equipped with a He-discharge lamp providing He–I photons of 21.22 eV for UPS analysis; and a monochromatic Al–Kα X-ray gun with photons energies of 1486.6 eV for XPS investigation.[39] The base vacuum of the system is ≈10^{-10} Torr. UPS He I measurements were performed to study the valence states of the prepared films. Vacuum level offsets were obtained from the shifts of the intensity thresholds at the lowest inelastic electrons kinetic energy cutoff, with a bias of –5.0 V with respect to ground. Position of the Fermi edge was calibrated using a clean Au film, and all spectra presented were plotted with respect to the determined Fermi level. All XPS measurements were calibrated with reference to the 4f 7/2 core level (83.98 eV) of a freshly sputtered Au film. Positions of the CB (or LUMO) levels of perovskite and C_{60} were estimated as 1.7 and 2.3 eV according to the charge transport gaps reported by measurements using inverse photoelectron spectroscopy.[6,40] For the vacuum-deposited sample, all organic films were thermally evaporated on an ITO glass substrate in a deposition chamber attached to the surface analysis system. The perovskite layer was prepared by coevaporation from $PbCl_2$ and MAI. The optimized mixing ratio of MAI and $PbCl_2$ was found to be ≈3:1. The sample was then annealed at 100 °C for 45 min. After cooled to room temperature, the sample was then transferred, without vacuum break, to the analysis chamber for UPS and XPS measurements. It was then transferred back to the deposition chamber for further deposition of C_{60}. After incremental C_{60} deposition, the sample was again analyzed with XPS and UPS. For the solution-processed sample, a $CH_3NH_3PbI_3$ precursor solution was prepared by dissolving MAI and PbI_2 into anhydrous N,N-Dimethylformamide at a MAI:PbI_2 = 1:0.7 molar ratio. The precursor solution was then spin coated onto an ITO glass substrate in a nitrogen-filled glove box, at 2000 rpm for 45 s. The film was left to dry at room temperature in the glove box for 30 min, to allow slow solvent evaporation. It was then annealed in the glove box at 100 °C for 15 min. The PCBM were dissolved in dichlorinebenzine at a concentration of 20–30 mg mL^{-1} and were spun on the perovskite layer followed by annealing for 10 min at 100 °C. The sample was then probed using photoemission study.

Device Fabrication and Measurement: Patterned ITO-coated glass substrates with a sheet resistance of 30 Ω/square were first cleaned with Decon 90, rinsed in deionized water, dried in an oven, and finally treated in an ultraviolet ozone chamber for 15 min.[41] All evaporating sources including MAI, C_{60}, Bphen are all (from Luminescence Technology Corp.) and $PbCl_2$ (form Aldrich) were used as received. The perovskite was prepared by coevaporation of $PbCl_2$ and MAI onto an ITO-coated glass substrate as described in the photoemission analysis. Deposition rates of $PbCl_2$ and MAI were monitored using two quartz crystal monitors, and the total thickness was monitored by another crystal monitor. After deposition of the perovskite layer, the sample is annealed at 100 °C for 45 min. The sample is then cooled to room temperature, and followed by depositing other organic layers. An Al cathode (80 nm) was deposited by thermal evaporation through a shadow mask. The active device area is 0.1 cm^2. The device was encapsulated in a glove box immediately after fabrication without ambient exposure. Performance of the device was measured with an Oriel 150 W solar simulator with AM1.5G (AM: air mass, G: global) filters at 100 mW cm^{-2}.

Supporting Information

Supporting Information is available from the Wiley Online Library or from the author.

Acknowledgements

The work described in this paper was supported by a grant from the Research Grants Council of the Hong Kong Special Administrative Region, China (Project No. T23–713/11) and the National Natural Science Foundation of China (No. 21303150 and No. 51473138).

Received: August 7, 2014
Revised: October 21, 2014
Published online: December 28, 2014

[1] M. M. Lee, J. Teuscher, T. Miyasaka, T. N. Murakami, H. J. Snaith, *Science* **2012**, *338*, 643.
[2] M. Liu, M. B. Johnston, H. J. Snaith, *Nature* **2013**, *501*, 395.
[3] J. Burschka, N. Pellet, S.-J. Moon, R. Humphry-Baker, P. Gao, M. K. Nazeeruddin, M. Grätzel, *Nature* **2013**, *499*, 316.
[4] L. Etgar, P. Gao, Z. Xue, Q. Peng, A. K. Chandiran, B. Liu, M. K. Nazeeruddin, M. Graetzel, *J. Am. Chem. Soc.* **2012**, *134*, 17396.
[5] H.-S. Kim, I. Mora-Sero, V. Gonzalez-Pedro, F. Fabregat-Santiago, E. J. Juarez-Perez, N.-G. Park, J. Bisquert, *Nat. Commun.* **2013**, *4*, 2242.
[6] P. Schulz, E. Edri, S. Kirmayer, G. Hodes, D. Cahen, A. Kahn, *Energy Environ. Sci.* **2014**, *7*, 1377.
[7] A. Marchioro, J. Teuscher, D. Friedrich, M. Kunst, R. van de Krol, T. Moehl, M. Grätzel, J.-E. Moser, *Nat. Photonics* **2014**, *8*, 250.
[8] T.-W. Ng, C.-Y. Chan, Q.-D. Yang, H.-X. Wei, M.-F. Lo, V. Roy, W.-J. Zhang, C.-S. Lee, *Org. Electron.* **2013**, *14*, 2743.
[9] B. Conings, L. Baeten, C. De Dobbelaere, J. D'Haen, J. Manca, H. G. Boyen, *Adv. Mater.* **2014**, *26*, 2041.
[10] Q. Chen, H. Zhou, Z. Hong, S. Luo, H.-S. Duan, H.-H. Wang, Y. Liu, G. Li, Y. Yang, *J. Am. Chem. Soc.* **2013**, *136*, 622.
[11] A. Abrusci, S. D. Stranks, P. Docampo, H.-L. Yip, A. K. -Y. Jen, H. J. Snaith, *Nano Lett.* **2013**, *13*, 3124.
[12] P. W. Liang, C. Y. Liao, C. C. Chueh, F. Zuo, S. T. Williams, X. K. Xin, J. Lin, A. K. Y. Jen, *Adv. Mater.* **2014**, *26*, 3748.
[13] J. Y. Jeng, Y. F. Chiang, M. H. Lee, S. R. Peng, T. F. Guo, P. Chen, T. C. Wen, *Adv. Mater.* **2013**, *25*, 3727.
[14] J. Y. Jeng, K. C. Chen, T. Y. Chiang, P. Y. Lin, T. D. Tsai, Y. C. Chang, T. F. Guo, P. Chen, T. C. Wen, Y. J. Hsu, *Adv. Mater.* **2014**, *24*, 4107.
[15] O. Malinkiewicz, A. Yella, Y. H. Lee, G. M. Espallargas, M. Graetzel, M. K. Nazeeruddin, H. J. Bolink, *Nat. Photonics* **2014**, *8*, 128.
[16] C. Wehrenfennig, G. E. Eperon, M. B. Johnston, H. J. Snaith, L. M. Herz, *Adv. Mater.* **2014**, *26*, 1584.
[17] F. Deschler, M. Price, S. Pathak, L. E. Klintberg, D.-D. Jarausch, R. Higler, S. Hüttner, T. Leijtens, S. D. Stranks, H. J. Snaith, M. Atatüre, R. T. Phillips, R. H. Friend, *J. Phys. Chem. Lett.* **2014**, *5*, 1421.
[18] Y. Yamada, T. Nakamura, M. Endo, A. Wakamiya, Y. Kanemitsu, *J. Am. Chem. Soc.* **2014**, *136*, 11610.
[19] C. S. Ponseca Jr., T. J. Savenije, M. Abdellah, K. Zheng, A. Yartsev, T. R. Pascher, T. Harlang, P. Chabera, T. Pullerits, A. Stepanov, *J. Am. Chem. Soc.* **2014**, *136*, 5189.
[20] H.-S. Kim, S. H. Im, N.-G. Park, *J. Phys. Chem. C* **2014**, *118*, 5615.
[21] H. Choi, J. Jeong, H.-B. Kim, S. Kim, B. Walker, G.-H. Kim, J. Y. Kim, *Nano Energy* **2014**, *7*, 80.
[22] S. D. Stranks, G. E. Eperon, G. Grancini, C. Menelaou, M. J. P. Alcocer, T. Leijtens, L. M. Herz, A. Petrozza, H. J. Snaith, *Science* **2013**, *342*, 341.
[23] J. Shi, J. Dong, S. Lv, Y. Xu, L. Zhu, J. Xiao, X. Xu, H. Wu, D. Li, Y. Luo, *Appl. Phys. Lett.* **2014**, *104*, 063901.
[24] H.-B. Kim, H. Choi, J. Jeong, S. Kim, B. Walker, S. Song, J. Y. Kim, *Nanoscale* **2014**, *6*, 6679.
[25] C.-H. Chiang, Z.-L. Tseng, C.-G. Wu, *J. Mater. Chem. A* **2014**,*2*,15897.
[26] P. Docampo, J. M. Ball, M. Darwich, G. E. Eperon, H. J. Snaith, *Nat. Commun.* **2013**, *4*, 2761.
[27] E. M. Miller, Y. Zhao, C. C. Mercado, S. K. Saha, J. M. Luther, K. Zhu, V. Stevanovi , C. L. Perkins, J. van de Lagemaat, *Phys. Chem. Chem. Phys.* **2014**, *16*, 22122.
[28] A.-L. Shi, Y.-Q. Li, Z.-Q. Xu, F.-Z. Sun, J. Li, X.-B. Shi, H.-X. Wei, S.-T. Lee, S. Kera, N. Ueno, *Org. Electron.* **2013**, *14*, 1844.
[29] E. Edri, S. Kirmayer, D. Cahen, G. Hodes, *J. Phys. Chem. Lett.* **2013**, *4*, 897.
[30] J. H. Noh, S. H. Im, J. H. Heo, T. N. Mandal, S. I. Seok, *Nano Lett.* **2013**, *13*, 1764.
[31] G. E. Eperon, V. M. Burlakov, P. Docampo, A. Goriely, H. J. Snaith, *Adv. Funct. Mater.* **2014**, *24*, 151.
[32] J. You, Z. Hong, Y. Yang, Q. Chen, M. Cai, T.-B. Song, C.-C. Chen, S. Lu, Y. Liu, H. Zhou, *ACS Nano* **2014**, *8*, 1674.
[33] L. E. Polander, P. Pahner, M. Schwarze, M. Saalfrank, C. Koerner, K. Leo, *APL Mater.* **2014**, *2*, 081503.
[34] B. P. Rand, D. P. Burk, S. R. Forrest, *Phys. Rev. B* **2007**, *75*, 115327.
[35] N. Li, B. E. Lassiter, R. R. Lunt, G. Wei, S. R. Forrest, *Appl. Phys. Lett.* **2009**, *94*, 023307.
[36] V. Mihailetchi, P. Blom, J. Hummelen, M. Rispens, *J. Appl. Phys.* **2003**, *94*, 6849.
[37] E. Edri, S. Kirmayer, S. Mukhopadhyay, K. Gartsman, G. Hodes, D. Cahen, *Nat. Commun.* **2014**, *5*, 3461.
[38] K. Tanaka, T. Takahashi, T. Ban, T. Kondo, K. Uchida, N. Miura, *Solid State Commun.* **2003**, *127*, 619.
[39] T. W. Ng, M. F. Lo, M. K. Fung, W. J. Zhang, C. S. Lee, *Adv. Mater.* **2014**, *26*, 5569
[40] M. F. Lo, T. W. Ng, H. W. Mo, C. S. Lee, *Adv. Funct. Mater.* **2013**, *23*, 1718.
[41] T. W. Ng, M. F. Lo, Q. D. Yang, M. K. Fung, C. S. Lee, *Adv. Funct. Mater.* **2012**, *22*, 3035.